

Intermetallic GaPd₂ Thin Films for Selective Hydrogenation of Acetylene

René R. Zimmermann,^[a] Martin Siebert,^[b] Shyjumon Ibrahimkutty,^[c] Roland Dittmeyer,^[b] and Marc Armbrüster*^[a]

Dedicated to Professor Juri Grin on the Occasion of his 65th Birthday

Abstract. The preparation of single-phase and catalytically active GaPd₂ coatings was accomplished via DC magnetron sputtering using an intermetallic sputter target. Thin and uniform layers were deposited on borosilicate glass, Si(111) and planar as well as micro-structured stainless steel foils. The specimens were examined regarding their phase composition, film morphology and microstructure. Thin films of different layer thickness were catalytically characterized in the semi-hydrogenation of acetylene, which was conducted at 473 K and a feed

gas composition of 0.5 vol.% C₂H₂, 5 vol.% H₂ as well as 50 vol.% C₂H₄ in helium. Pre-reduction of the catalyst was found to be essential to enhance the catalytic selectivity. Sputtered GaPd₂ showed a high selectivity of 73 % for the hydrogenation to ethylene at conversion levels above 80 %. The surface-specific activity was strongly increased to 8.97 mol_{acetylene}·(A₀·h)⁻¹ compared to bulk- or nanoscale GaPd₂ (1.93 and 0.30 mol_{acetylene}·(A₀·h)⁻¹, respectively) caused by the high specific surface area of the thin films.

Introduction

Heterogeneously catalyzed selective hydrogenations are important reactions, which are applied in several industrial processes. One process with global relevance is the production of high-purity ethylene, which is further used as feedstock for polyethylene or ethylene oxide synthesis. Polyethylene is with an annual production of 70 million tons in 2010 the most produced polymer and has an expected annual growth of 3%.^[1] The ethylene-enriched gas mixture originating from steam cracking of the naphtha fraction contains 0.5 to 2 vol.% acetylene, which poisons the catalyst of the subsequent polymerization reaction.^[2] Therefore, the separation or conversion of acetylene below 2 ppm is essential.^[3] The latter is economically reasonable, as both, the quality and quantity of ethylene is increased using this approach. State-of-the-art catalysts con-

sist of well-dispersed palladium alloys like Ag-Pd or Au-Pd on a support material – e.g. α -Al₂O₃.^[4] The disadvantage of those catalysts is an occurring segregation effect under reaction conditions, whereby the catalytically active sites, and thus the selectivity, change with time. Additionally, the formation of palladium hydrides is observed for the alloyed systems, which is drastically decreasing the ethylene selectivity.^[5]

In recent years, there was comprehensive research about intermetallic compounds and their application as catalysts.^[6] In contrast to alloys intermetallic compounds possess a well-ordered crystal structure causing different and unique material properties. In the case of selective hydrogenation reactions, the resulting strong active-site isolation with limited segregation effects is beneficial for the selectivity. For the selective hydrogenation of acetylene, intermetallic Ga-Pd compounds are highly active and selective site-isolated catalysts, which show no formation of Pd-hydrides.^[7] Bulk intermetallic compounds in this system are formed by melting the corresponding amounts of gallium and palladium, followed by annealing and grinding of the obtained materials. Among those compounds, GaPd₂ shows the most promising properties, combining a high selectivity for the semi-hydrogenation of acetylene of about 75 % at conversion levels above 90%.^[6a] Due to the low specific surface area of the bulk material a synthesis route to prepare GaPd₂ nanoparticles was developed.^[8] The obtained nanoparticles have particle sizes of 2–10 nm and show a very high specific surface area of ca. 40 m²·g⁻¹, which results in a 35,000-fold higher specific activity compared to bulk-GaPd without forfeiting the good selectivity.

Investigation of the catalytic performance of these highly active catalysts in conventional chemical reactors is challenging due to the high exothermicity of the hydrogenation reaction. A well-known issue in this context is the sintering of

* Prof. Dr. M. Armbrüster

E-Mail: marc.armbruester@chemie.tu-chemnitz.de

[a] Materials for Innovative Energy Concepts


Institute of Chemistry
Faculty of Natural Sciences
Chemnitz University of Technology
09107 Chemnitz, Germany


[b] Institute for Micro Process Engineering (IMVT) and Institute of Catalysis Research and Technology (IKFT)

Karlsruhe Institute of Technology
Hermann-von-Helmholtz-Platz 1
76344 Eggenstein-Leopoldshafen, Germany

[c] Max Planck Institute for Solid State Research

Heisenbergstr. 1
70569 Stuttgart, Germany

 Supporting information for this article is available on the WWW under <http://dx.doi.org/10.1002/zaac.202000124> or from the author.

 © 2020 The Authors. Published by Wiley-VCH Verlag GmbH & Co. KGaA. • This is an open access article under the terms of the Creative Commons Attribution License, which permits use, distribution and reproduction in any medium, provided the original work is properly cited.

the catalytically active material due to hot-spot formation. In contrast to conventional plug-flow reactors, micro-structured reactors are characterized by a very high surface-to-volume ratio, which provides excellent heat and mass transport properties to overcome the limitations owing to the fast and highly exothermic reaction.^[9] To allow for process intensification, a controlled and homogeneous application of the catalytic material inside the micro-structured reactor is required, which is mostly realized by preparing a micro-fixed bed or surface coating. The lower pressure drop as well as reduced sintering and segregation of catalyst coatings are advantageous compared to the use of micro-fixed beds.^[10]

Convenient designs of laboratory micro-structured reactors for catalytic investigations contain a single micro-structured metal foil up to a stack of foils.^[11] These open micro-structures can be produced by etching or milling of a flat metal substrate, which generates multiple, parallel and well-defined micro-channels. Several techniques like dip coating, sol-gel-methods or screen printing have been demonstrated as being practicable for coating of laboratory scale micro-channel reactors. However, these methods often showed certain limitations like poor uniformity and reproducibility if a multitude of channels is covered. Additionally, undesired coating on top of the fins and side bands of the micro-structures occurs. Recently, the use of drop-on-demand inkjet-printing for depositing GaPd₂ nanoparticles into micro-structured channels was demonstrated.^[12] Common to all the mentioned techniques is the limitation to produce very thin coatings with a thickness below 1 μm. DC magnetron sputtering represents an alternative to overcome this constraint. It obviates the need for the complex and time-consuming synthesis of GaPd₂ nanoparticles, which is an integral part of all the aforementioned coating procedures. Further, it is possible to coat surfaces more efficiently and with lower amounts of intermetallic material. Sputter deposition generates very dense and compact coatings with a good reproducibility and well-scalable thicknesses ranging from a few nanometers to several micrometers. Further advantages of magnetron sputtering are the absence of organic solvents in the process and thereby avoiding liquid waste, lower material costs compared to other coating techniques and the possibility of applying screens to perform the coating of multiple patterns (e.g. deposition only into the channels but not onto the fins between each channel). An example for thin film deposition of catalytically active systems is the sputtering of Pd₉₀Au₁₀ and GaPd on top of CuPd membranes, which was applied for the direct hydroxylation of benzene to phenol.^[13] Furthermore, the sputtered alloy-based system Au-Pd was investigated by Guo and co-workers for the oxidation of benzyl alcohol as well as benzylamine.^[14]

Reports on successful sputtering of single-phase intermetallic compounds are rare. There have been publications on complex intermetallic compounds like Al₄(Cr,Fe)^[15] or β-Al(Cu,Fe),^[16] and some results for sputtering of simple bi-metallic compounds with an equimolar atomic ratio and just two atoms in the unit cell like FeCo.^[17] But up to now, there are no reports in literature about the successful sputtering of single-phase intermetallic GaPd₂. For instance, Kim et al. used

electronic beam evaporation to deposit Pd on a GaN surface. Subsequent annealing at 973 K for 30 s led to the formation of a mixture of Ga₂Pd₅ and Ga₅Pd intermetallic compounds.^[18] Grodzicki et al. sputtered a 1.5 nm thick Pd layer on a defined GaN surface. Annealing at 823 and 1073 K initiated the formation of island-type conglomerates of GaPd₂ and GaPd, respectively.^[19] Furthermore, Mayr et al. thermally evaporated Ga and Pd by turns on a Ta sheet and subsequently annealed at 673 K. The obtained 400 nm thick layer showed a slightly Pd-enriched bulk-GaPd₂ including the neighboring phase Ga₅Pd₁₃ as minor impurity.^[20] According to the deposition techniques shown, the resulting layers were mixtures of a main phase and mostly one neighboring phase.

The objectives of the present work include the synthesis of an intermetallic sputter target, the deposition of thin intermetallic GaPd₂ layers via DC magnetron sputtering and the evaluation of their catalytic properties in the selective hydrogenation of acetylene. Overall, the main challenge is to produce single-phase intermetallic coatings via sputtering, because only the intermetallic phase will provide the desired catalytic properties.

Results and Discussion

Sputter Target Engineering

The preparation of an intermetallic sputter target of GaPd₂ was necessary, as there are no intermetallic sputter targets commercially available. Commercial targets were not single-phase or contained just stoichiometric mixtures of the constituent elements. Pre-requisite for the synthesis of intermetallic sputter targets are high-purity base materials, which is here the intermetallic compound GaPd₂. The single-phase nature was proven by powder X-ray diffraction (pXRD) (Figure S1, Supporting Information).

The subsequent synthesis of the intermetallic sputter target was carried out by spark plasma sintering (SPS) from powdered bulk-GaPd₂. All sinter experiments were conducted in vacuum to avoid oxidation during the high-temperature treatment. Test samples with a diameter of 10 and 25 mm were successfully synthesized. After optimizing the sintering parameters, well-compacted samples with 97.6% of the crystallographic density were obtained. The mechanical stability of the small sintered samples was sufficient for the metallographic preparation of cross sections. Optical as well as scanning electron micrographs were taken to get further information on the compacting behavior and homogeneity of the sintered samples (Figure S2, Supporting Information). Another part of each sample was crushed and analyzed concerning phase composition, where solely the reflections of GaPd₂ could be detected in the respective X-ray diffraction pattern. As thermal expansion was expected to occur in the target during the sputter experiments, the stability of the target had to be enhanced by a supporting layer. Freshly polished 3 mm thick copper discs were used to increase the stability and heat conductivity of the sputter target, which is in total 6 mm thick. Sinter experiments of small test samples showed the same compacting behavior as

without a supporting disc. This was concomitant with a partial reaction of the intermetallic compound with the copper resulting in diffusion layers of 80 μm with three ternary Cu-Ga-Pd compounds (Figure S3, Supporting Information). Their composition was determined by energy dispersive X-ray spectroscopy (EDX), which revealed that the diffusion direction goes from copper into GaPd₂. These 80 μm regions are tolerated, as the total intermetallic layer thickness of 3 mm is much higher. Thereby sputtering of the binary intermetallic compound is guaranteed for the major part of the sputter target.

Graphite foils were used to encase the test samples and final target during the sinter experiments, which afterwards strongly adhered to the sintered samples. Subsequent polishing removed the graphite foil. The single-phase nature of the final target was verified by pXRD in Bragg–Brentano geometry. The most intense reflections of GaPd₂ were observed in the sintered target and all reflections could be assigned to this intermetallic compound.

DC Magnetron Sputtering

Thin, compact and uniform GaPd₂ layers were successfully deposited on borosilicate glass, Si(111) and stainless steel via DC magnetron sputtering using the intermetallic target. Both hydrogen and argon plasma were successfully ignited and glowed very stable for the considered magnetron powers of 80–140 W and operating pressures p_{Ar} of 0.4–1.2 Pa. During initial usage of the target, it was required to sputter for 1 h without deposition using a shield in front of the substrate until a stable magnetron voltage was reached. After that, only short pre-sputter times of 3–15 min were necessary to equilibrate the target for changed operation settings. Initially, the deposition rate was determined by sputtering of samples on glass discs applying different argon partial pressures and sputter times. The layer thickness was calculated based on the weight gain of the samples, which was converted into deposition rates. Deposition rates obtained from different sputter parameters are given in Table 1.

Table 1. Deposition rates for different DC magnetron powers and argon partial pressures using an intermetallic GaPd₂ target. During deposition, the substrate was biased with 80 V.

$P_{\text{Magnetron}} / \text{W}$	$p_{\text{Ar}} / \text{Pa}$	$r(\text{GaPd}_2) / \text{nm}\cdot\text{min}^{-1}$	$r'(\text{GaPd}_2) / \text{nm}\cdot(\text{min}\cdot\text{kW})^{-1}$
100	0.4	18(1)	185(9)
100	0.8	20(2)	195(16)
100	1.0	20(2)	195(19)
140	0.8	29(3)	204(24)
80	0.8	16(4)	196(53)

The deposition rates $r(\text{GaPd}_2)$ show marginal dependency on the argon partial pressure. Increasing the DC magnetron power leads to an increased deposition rate. For a better comparison, the normalized deposition rate $r'(\text{GaPd}_2)$ per time (min) and power (kW) is introduced. Their values show that the normalized deposition rate $r'(\text{GaPd}_2)$ can be approximated to be constant at argon partial pressures in the range of 0.4–1.0 Pa and DC magnetron powers of 80–140 W. For the depo-

sition of the catalytically active layers inside the micro-structured channels, a magnetron power of 100 W and an argon partial pressure of 1.0 Pa was chosen, which corresponds to a deposition rate of 20(2) $\text{nm}\cdot\text{min}^{-1}$. The relatively high standard deviation of the deposition rates is due to the decreasing layer thickness with increasing distance from the target. For each deposition experiment, two glass discs (to quicker determine the standard deviation) were mounted on the rotatable substrate holder in front of the sputter target at a distance of 60 mm. The spatial alignment of the substrates leads to small deviations of the final layer thickness depending on the local position. The influence of this effect is minimized by reducing the amount of substrates per experiment and their arrangement directly side by side.

Subsequent optical examination of the micro-structured foils after deposition shows a uniform and smooth, metallic-silverish coating over the entire sputtered area. Due to the expected high catalytic activity of the GaPd₂ thin films, the micro-structured foils were partially shielded with aluminum foil leaving only a small slit in the middle of each foil in the range of 1–1.5 mm situated for deposition of GaPd₂. This procedure works well, but during assembly of the partly covered micro-structured foils on the substrate holder, a slight shift of the aluminum foil could not be excluded. This leads to a small deviation of the desired coating-width in the range of 0.1 mm, limiting the accuracy of the calculated catalytic activity.

Thin Film Characterization

Shiny, silverish thin films of GaPd₂ were obtained on all tested substrates, which were borosilicate glass discs, Si(111) single crystals as well as planar and micro-structured stainless steel foils. All films had metallic luster, appeared optically homogeneous and had no faint shadows. Thin films were firstly sputtered on amorphous borosilicate glass to determine GaPd₂ deposition rates $r(\text{GaPd}_2)$ and $r'(\text{GaPd}_2)$ because this is the thinnest and lightest substrate, which is ideal for weighing purposes. Thereafter, the phase composition was analyzed by powder X-ray diffraction (pXRD) in the as-sputtered state (Figure S4, Supporting Information). The diffraction pattern was background corrected as the amorphous glass substrate causes a broad and intense signal at low diffraction angles.

Nevertheless, all reflections can be assigned to the crystal structure of GaPd₂.^[21] As glass is a brittle substrate, the following step was coating of more stable substrates. Si(111) single-crystalline slabs are much more mechanically stable than glass, they are easy to cut and possess a highly ordered surface. Firstly, the deposited layer was investigated by pXRD and grazing incidence X-ray diffraction (GIXRD) regarding its phase composition, where the obtained reflections were assigned to intermetallic GaPd₂ (Figure 1). The angle of incoming X-rays (ω) was varied between 0.2 and 10° to analyze the surface and bulk composition, respectively. There are partially significant differences between the calculated and experimentally observed reflection intensities for different ω values, which could be caused by a (210) preferred orientation of the thin films. Some reflections are even entirely missing in the

powder diffraction pattern. Another reason for odd reflection intensities could be the fixed position of the sample because there was no possibility to rotate the samples during the measurement. Thus, the sample might be not statistically orientated and examined. Additionally, electron backscatter diffraction (EBSD) was applied to reveal a preferred orientation of the thin films. This failed most likely due to the low film thickness and is still under investigation on thicker films.

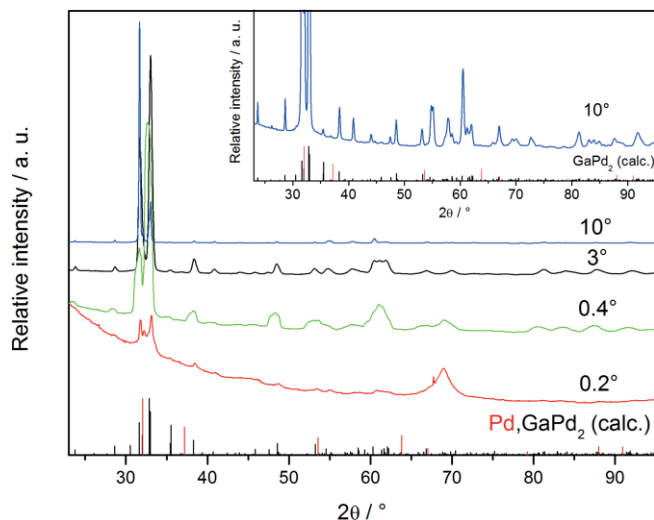


Figure 1. GIXRD pattern of GaPd₂ sputtered on Si(111) for different incident angles (ω) and calculated powder pattern of GaPd₂.^[21] An enlarged diffraction pattern for $\omega = 10^\circ$ is shown in the inset. Calculated GaPd₂ film thickness 1050 nm.

The main phase for all incoming angles is GaPd₂. Nevertheless, elemental palladium cannot be fully excluded in the most surface sensitive powder diffraction pattern ($\omega = 0.2$) due to partially identical positions of the most intense reflections.

The top view of a GaPd₂ thin film as-sputtered on Si(111) exhibits a flat and homogeneous surface that contains some randomly distributed holes (Figure 2). EDX analysis and elemental mapping were conducted on a cross section of GaPd₂/Si(111) to prove the elemental composition as well as a homogeneous distribution of Ga and Pd in the thin film. According to EDX spectra, the thin film has the formula GaPd_{2.2(2)}, which confirms the expected composition. Elemental mapping was done for gallium, palladium and silicon to verify a homogeneous distribution of Ga as well as Pd in the thin film and for exclusion of significant reactions of the sputtered layer with the Si(111) substrate. According to EDX analysis, no preferred deposition of Ga or Pd was detected (Figure 3). Instead, there is a sharp boundary of the intermetallic layer and the substrate, which confirms that no substantial reactions occurred during the sputter process. Thus, crystal structure, chemical composition and elemental distribution for thin films deposited on Si(111) turned out as expected for intermetallic GaPd₂. The substrate was accordingly changed from the model system silicon to stainless steel, which is the aimed-for substrate for the subsequent catalytic investigations.

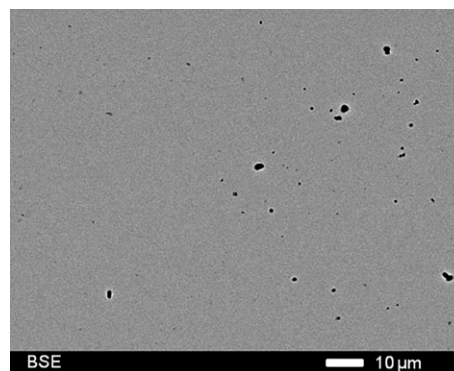


Figure 2. Top view (electron micrograph) of a GaPd₂ layer grown on Si(111) at 100 W magnetron power and 80 V bias voltage.

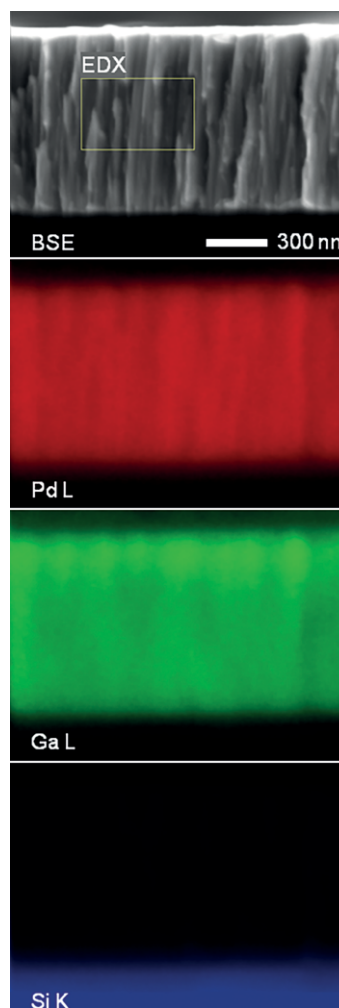


Figure 3. EDX mapping of a cross section of GaPd₂ on Si(111). The box in the BSE image represents the area that was used for EDX compositional analysis presented in the text.

Thin films were deposited on stainless steel and initially investigated by GIXRD regarding their phase composition. The incident angle (ω) was similarly varied between 0.2 and 10° to analyze the surface and bulk composition, respectively. The GaPd₂ reflections overlap especially at low incident angles

partially strongly but most of the obtained reflections could be assigned to intermetallic GaPd₂ (Figure 4). Additional reflections that are caused by the stainless steel substrate are more prominent for higher ω values as these measurements are more bulk sensitive. As already observed for GaPd₂ on Si(111), there are partially significant differences between the calculated and experimentally observed reflection intensities.

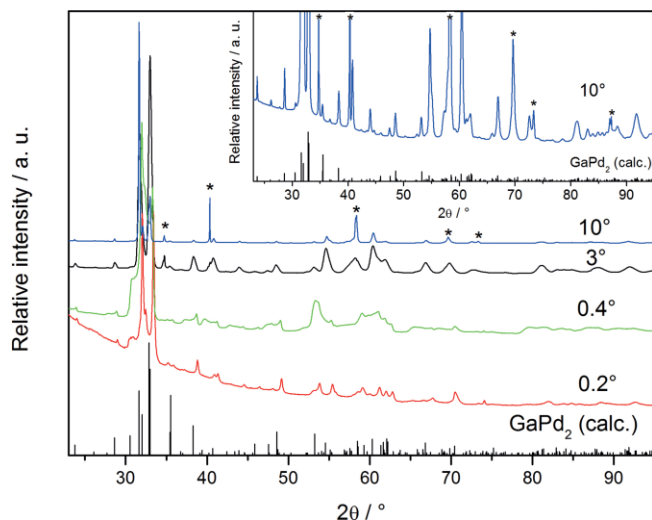


Figure 4. GIXRD pattern of GaPd₂ sputtered on planar stainless steel for different incident angles (ω) and calculated powder pattern of GaPd₂.^[21] An enlarged diffraction pattern for $\omega = 10^\circ$ is shown in the inset. Asterisks denote reflections of the stainless steel substrate. Calculated GaPd₂ film thickness 2280 nm.

Here, these differences are less pronounced but the reason for this might be a preferred orientation of the thin films, too. Due to the higher resolution of GIXRD data in contrast to GaPd₂/Si(111), elemental palladium can be excluded in all powder diffraction patterns. Furthermore, there are no indications for other Ga-Pd phases or oxides in the GIXRD patterns, whereby the thin film on the stainless steel foil is single-phase GaPd₂. Phase composition was also analyzed in the as-sputtered and annealed state for 20, 40 and 60 nm thick films, which were later catalytically investigated. All samples showed in as-sputtered state just two reflections that are caused by the stainless steel substrate. After annealing at 723 K for 4 h in flowing Ar/H₂, three reflections appeared for the 40 and 60 nm samples (Figure S5, Supporting Information). Due to the very thin layer and thereby expected low intensities, there are still no reflections for the 20 nm thin film (not shown). The detected reflection positions can be explained by the most intense reflections of the GaPd₂ crystal structure.

The microstructure of thin films deposited on stainless steel was investigated from top and on a cross section to verify ideally the same properties like on Si(111). Figure 5 shows a top view of GaPd₂ on planar steel and reveals a flat and homogeneously appearing surface. In contrast to layers on silicon, there were no holes visible on the surface. The micrograph of a cross section of GaPd₂ inside of a micro-structured foil (Figure 6) reveals a dense and homogeneous layer. The rough surface of the GaPd₂ layer in Figure 6 could be due to the

intrinsic roughness of the etched microstructured channels. Attempts to evaluate the specific surface area of the films by electron microscopy and X-ray diffraction failed due to the thin nature of the films as well as the structuring of the foils. Characterization of the films on the flat substrates revealed very smooth surfaces (within an estimated roughness of 5 to max. 10 nm), suggesting the use of the geometric surface area resulting in an upper limit for the surface specific activity. EDX analysis revealed a composition of GaPd_{2.0(1)} on planar steel as well as inside of the micro-structured stainless steel foils. This is in full agreement with the expected composition of GaPd₂ as well as the thin films on Si(111). Hence, intermetallic GaPd₂ thin films were successfully grown on borosilicate glass, Si(111) and stainless steel, which enables catalytic investigations on a well-defined intermetallic compound.

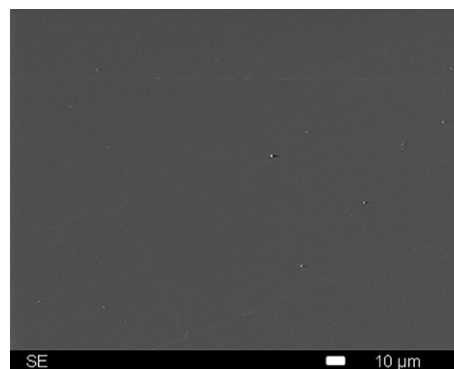


Figure 5. Top view (electron micrograph) of a GaPd₂ layer grown on planar stainless steel at 100 W magnetron power and 80 V bias voltage.

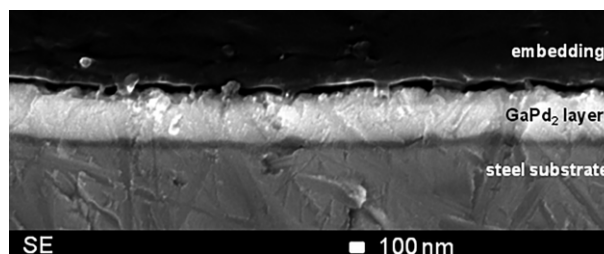


Figure 6. SEM micrograph of the cross section of a GaPd₂ coating on the bottom of a micro-structured channel of a stainless steel substrate.

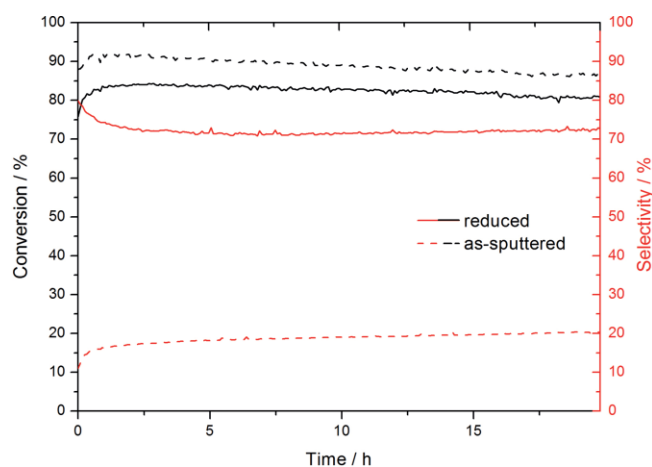
Catalytic Testing

The sputtered layers were firstly catalytically investigated in the selective hydrogenation of acetylene without any pre-treatment. This was based on experience with bulk-GaPd₂, where reduction is not necessary to exhibit 75% selectivity at conversion levels of 90–95%.^[8] The as-sputtered sample shows at high conversion of slightly below 90% only a poor selectivity of 20% (Figure 7), which reminds of supported elemental or alloyed Pd catalysts.^[8] As elemental palladium cannot be fully excluded, this could be one reason for such a low selectivity. According to previous investigations of bulk- and printed GaPd₂, a pre-reduction step at 723 K for 4 h with

Table 2. Catalytic performance of GaPd₂ catalyst materials compared to 5% Pd/Al₂O₃.^[8,12]

Catalyst	Conversion / %	Selectivity / %	$n_{\text{Pd}} / \text{mmol}$	Activity / $\text{mol}_{\text{acetylene}} \cdot (\text{mol}_{\text{Pd}} \cdot \text{h})^{-1}$	Activity / $\text{mol}_{\text{acetylene}} \cdot (\text{A}_0 \cdot \text{h})^{-1}$
Bulk-GaPd ₂ [8]	94.7	75	7.08×10^{-2}	5.44	1.93
Nano-GaPd ₂ /Al ₂ O ₃ [8]	86.5	67	5.17×10^{-5}	7.12×10^3	0.30
printed GaPd ₂ /Al ₂ O ₃ [12]	91.8	76	7.82×10^{-4}	4.80×10^2	0.13
Sputtered GaPd ₂ 20 nm	41.1	72	4.31×10^{-5}	3.93×10^3	8.97
Sputtered GaPd ₂ 40 nm	39.8	74	8.62×10^{-5}	1.90×10^3	8.69
Sputtered GaPd ₂ 60 nm	36.1	71	1.29×10^{-4}	1.15×10^3	7.88
5% Pd/Al ₂ O ₃ [8]	44.9	17	7.05×10^{-5}	2.45×10^3	0.21

5 vol.% H₂ in Ar was conducted prior to the catalytic test.^[12] This treatment could remove thin oxide layers from the material as well as improve the atomic arrangement within the sputtered films. The beneficial effect of this pre-treatment is revealed by a catalytic test resulting in a selectivity of 73% at 82% conversion, which is very close to that of bulk-GaPd₂ (Figure 7).

**Figure 7.** Catalytic properties of GaPd₂ thin films at 200 °C in the as-sputtered state and after reductive pre-treatment for 4 h at 450 °C.

The specific activity of the thin films was determined by covering the same area of three different micro-structured foils with 20, 40, and 60 nm layers of intermetallic GaPd₂, respectively. The obtained conversion after 20 h time on stream is in a close range for the three different layer thicknesses (Table 2). Deviations from this will be mainly caused by the limited but still high precision of the partial shielding of micro-structured channels with aluminum foil during thin film deposition. Based on the different total amount of palladium (n_{Pd}) within the 20, 40, and 60 nm thick layers, having a proportion of 1 : 2 : 3, the expected mass-specific activities of those layers should have a ratio of 1 : 0.5 : 0.333. The actual ratio (based on the values in Table 2) of 1 : 0.48 : 0.29 is in good agreement to our expectation and confirms the high precision of this coating approach. The surface-specific activity should be independent of the layer thickness if the sputtered area would be the same for all foils. As for the mass-specific activities the surface-specific activities are very similar whereby the expected behavior could be proven.

Very surprisingly, the surface-specific activities of these three foils are about 30 times higher than for nanoparticulate GaPd₂/Al₂O₃, which possesses the highest activity (per amount

of Pd) of the compared systems. The first reason for the big difference between sputtered foils and nanoparticulate GaPd₂ is the surface area, which is actually accessible for the catalytic conversion. In case of the sputtered foils, this equals exactly the calculated surface area and neglects the influence surface roughness on the nanometer scale, thus, these values represent upper limits of the surface-specific activity. In contrast, for the nanoparticles large parts of the surface are inaccessible because of the contact to the support. Additionally, agglomerates with enclosed GaPd₂ nanoparticles are not doing catalysis, either. According to these points, it was estimated that the catalytically accessible surface is just half of the total nanoparticle surface, which would at the same time double their surface-specific activity. The major reason for the huge difference between nanoparticles and the sputtered layers can be addressed to structural differences of the nanoparticle surface, which do not possess the ideal intermetallic structure like bulk GaPd₂ or the sputtered layers.^[22] This is accompanied by strong surface coverage with gallium oxides, which is another explanation for the higher surface-specific activity of the sputtered layers.^[22] Finally, the potential (210) preferred orientation of the sputtered films could have led to the increased activity as well. This option is evident because it is well-known that the catalytic activity and selectivity can vary drastically on different surfaces of the same intermetallic compound.^[23] Thus, this surface might be more active than the statistically orientated bulk material.

The different dimensions of 7 and 20 nm for nanoparticulate and sputtered GaPd₂, respectively will cause higher mass-specific activity of the nanoparticulate sample. Going to even thinner films should invert this behavior, which emphasizes the great potential of thin film coatings like GaPd₂ for their application as catalytically active material and might be used for other catalytic reactions as well. Due to technical limitations of the used sputter device thinner films could not be synthesized with the same set of sputter parameters. These parameters should be kept as changes could affect the layer properties.

Conclusions

Thin films of the intermetallic compound GaPd₂ were successfully deposited as single phase on several substrates by DC magnetron sputtering. The crystal structure of GaPd₂ was confirmed on all substrates and in as-sputtered as well as pre-reduced state. Varying reflection intensities could be caused by a preferred orientation during thin film deposition. Differences

of the phase composition were pronounced for very thin films ≤ 60 nm, as the powder diffraction pattern after annealing at 723 K for 4 h revealed reflections that could be assigned to intermetallic GaPd₂. The layers are very dense and homogeneous. Differences between the thin films are the higher number of holes for GaPd₂ on Si(111) and the microscopically detected higher surface roughness for layers inside of the etched micro-structured reaction channels. Elemental composition of the layers was determined by EDX measurements, which approved the expected composition of GaPd₂. Subsequent EDX mappings showed homogeneous distribution of Ga as well as Pd in the thin film and endorsed the absence of reactions between substrate and the intermetallic layer. Catalytic tests were conducted on thin films that were grown in micro-structured reaction channels. The limited selectivity of as-sputtered GaPd₂ proved a pre-reduction step to be necessary prior to the catalytic experiments. This resulted in 73% selectivity, which is very close to that of bulk-GaPd₂. Small deviations from the calculated values for activity per amount of palladium and surface area were related to preparation accuracy. The highest activity per mol_{Pd}·h of the presented thin films (obtained on sputtered GaPd₂ 20 nm) is around 700 times higher than bulk material, while the activity per surface area is for all thin films about 4 and 30 times higher than values for bulk- and nano-GaPd₂, respectively. Films < 20 nm should have the potential to outperform even the most active Ga-Pd catalyst material reported in literature.^[8]

Experimental Section

Sputter Target Synthesis: GaPd₂ was synthesized as described previously by melting the appropriate amounts of gallium (ChemPur, 99.9999%) and palladium (KOOS Edelmetalle, 99.95%) in a high-frequency furnace (Hüttinger TIG 5/300) in an argon atmosphere and subsequent annealing in evacuated quartz glass ampoules for 10 d at 1073 K in batches of 20 g.^[24] The phase composition of each batch was analyzed by powder X-ray diffraction (pXRD) on an image plate Guinier camera G670 (Huber) with CuK_{α1} radiation ($\lambda = 1.540598$ Å) and a Ge(111) monochromator.

The compacting of the intermetallic sputter target was carried out by spark plasma sintering (SPS) from powdered bulk-GaPd₂. Test samples were synthesized on a 515 ET (Syntex-Fuji) and had a diameter of 10 as well as 25 mm. The final sputter targets, which were synthesized on a HP D 250C (FCT Systeme) possessed a diameter of 100 mm. The experiments were carried out under vacuum at a background pressure of less than 10 Pa. All samples were sintered on a freshly polished 3 mm thick oxygen-free copper disc (Allmeson, $\geq 99.95\%$) of the same diameter enhancing the stability and heat transport of the target, which had a total thickness of 6 mm in the end. All SPS experiments were conducted in appropriate graphite dies using graphite punches to apply uniaxial pressure and graphite foil on all sides to isolate the sinter samples from the punches as well as the dies. For the final sputter target, the loaded die was heated to 673 K with 29 K·min⁻¹ whereafter a force of 48 kN (equal to a pressure of 30 MPa) was applied. While keeping this pressure, the temperature was raised to 1223 K with 29 K·min⁻¹ and held for 60 min. The graphite foil was removed after sintering by manual polishing with silicon carbide paper. Cross sections of the test specimens were produced by an Accutom-

50 cut-off machine (Struers) and subsequently investigated for the compacting grade and possible reactions of the copper plate with intermetallic GaPd₂ using an Axioplan 2 optical microscope (Zeiss) in bright field and with polarized light. The grade of compacting was determined by weighing the sample in ethanol and in air in the following way:

$$\rho_{\text{arch}} = \frac{\rho_{\text{EtOH}}(T) m_{\text{air}}}{m_{\text{air}} - m_{\text{EtOH}}} \quad (1)$$

$$\text{Grade of compacting} = \frac{100\% \rho_{\text{arch}}}{\rho_{\text{IMC}}} \quad (2)$$

where ρ_{arch} , $\rho_{\text{EtOH}}(T)$, and ρ_{IMC} are the archimedean density, the temperature dependent density of ethanol, and the density of intermetallic GaPd₂. The sample mass in air and in ethanol are denoted as m_{air} and m_{EtOH} .

Phase composition of the synthesized sputter target was analyzed by pXRD in Bragg–Brentano geometry on a STADI MP diffractometer (STOE) with CuK_{α1} radiation ($\lambda = 1.540598$ Å) and a Ge(111) monochromator.

DC Magnetron Sputtering: Different materials were used as substrate for the coating, namely: silicon (CrysTec, (111), CZ, *p*-type, boron doped, polished), circular borosilicate glass discs (VWR, Mat. No.: 631–0172) as well as planar and micro-structured stainless steel foils (Ätztechnik Herz, 1.4404). If the micro-structured foils should only be partially coated, aluminum foil (ROTH Rotilabo, Al > 99%) was used to protect those parts where no deposition should occur.

The PVD/CVD device STARON 6060 (PT&B Silcor) was used for DC magnetron sputtering. The sputter target was installed vertically into the vacuum chamber. The target was mounted on a copper plate at the chamber wall for improved heat conduction to the cooling system on the back side ($T_{\text{water}} = 291$ K). The substrate was connected to a rotatable substrate holder and aligned parallel to the target at a distance of 60 mm. Vacuum below 5×10^{-4} Pa was achieved using a rotary valve pump (TRIVAC D65B), a roots pump (RUVAC WSU 501 H) and a turbo molecular pump (TURBOVAC T1600). During the evacuation, the chamber was heated to 573 K for 30 min to improve the removal of adsorbed species. After reaching the final vacuum, a glow discharge cleaning was performed to remove impurities from the surfaces of target, substrate holder and substrate. For this, a hydrogen plasma (Air Liquide, 99.999%) was ignited and the substrate holders were biased with a voltage ramp from 80 to 160 V and passed the plasma several times until the measured current field was constant. After that, a pre-sputtering step was conducted to remove any residual species from the target surface (e.g. oxide layers) and to equilibrate the plasma until a constant deposition rate was reached. For this, pure argon (Air Liquide, 99.999%) was supplied to the vacuum chamber at a flow rate of 200 mL·min⁻¹ and Ar partial pressure as well as magnetron power were set as required for the subsequent sputter deposition. During the pre-sputtering, the substrate was covered by a shield to avoid contamination. After reaching constant conditions, the shield was removed and the substrate holder was biased with 80 V during the whole sputter deposition to improve coating adhesion. An overview of the used parameters for all steps is given in Table 3. To determine deposition rates, films with masses of 1.371–2.562 mg were deposited and weighed with an accuracy of 0.001 mg.

Post-Treatment: The sputtered specimens were annealed exactly like the reduction step before each catalytic experiment. This was conducted in 40 mL·min⁻¹ flowing Ar/H₂ (5 vol.% H₂ in argon

Table 3. Overview of DC magnetron sputter algorithm and main parameters for obtaining intermetallic GaPd₂ coatings.

Step	<i>t</i> /min	<i>U</i> _{BIAS} / V	<i>P</i> _{Magnetron} /W	Sputter gas	<i>p</i> / Pa
Plasma cleaning	10	80–160	100	H ₂	0.8
Pre-sputtering	30	–	100	Ar	0.8
Sputtering	1–3 ^{a)}	80	100	Ar	0.8

a) Sputter times used for coating of micro-structured foils. Sputter times to obtain thicker or thinner layers for characterization purposes were adjusted accordingly.

(> 99.998 %) in a quartz glass tube. The tube was evacuated before and after each annealing to avoid oxygen contamination during the heat treatment. The annealing temperature was set to 723 K, which was held for 4 h applying heating as well as cooling rates of 5 K·min⁻¹. After cooling to room temperature, the samples were stored in vacuum until they were further analyzed.

Characterization of Sputtered Layers: Phase composition of the sputtered layers was firstly determined by pXRD on an image plate Guinier camera G670 (Huber) and in Bragg–Brentano geometry, respectively. The fixed angle ω of the incoming beam was varied between 2 and 14.4° depending on the thickness of the sputtered layer. Additionally, exemplary samples were investigated by grazing incidence X-ray diffraction (GIXRD) at the MPI beamline at the synchrotron “Angström Quelle Karlsruhe“ (ANKA) in a helium flushed dome.^[25] The GIXRD measurements were conducted using a monochromatic photon energy of 10 keV, which corresponds to $\lambda = 1.239842 \text{ \AA}$.

Microstructural arrangements of the sputtered layers were investigated on cross sections and top views by a JSM-7800F (JEOL) scanning electron microscope (SEM), which is equipped with a QUANTAX 400 EDX system (Bruker). The deposition rates $r(\text{GaPd}_2)$ at various argon partial pressures were calculated by the following equation:

$$r(\text{GaPd}_2) = \frac{4 m(\text{GaPd}_2)}{\pi \rho(\text{GaPd}_2) d^2 t} \quad (3)$$

where $m(\text{GaPd}_2)$ is the mass of deposited GaPd₂ that was sputtered on a circular area with the diameter d . The deposition time and the crystallographic density of GaPd₂ are indicated by t as well as $\rho(\text{GaPd}_2)$. For this, the weight gain of borosilicate glass probes was measured after the sputter process. Knowing the density of the layer and the sputtered area allows for calculating the height of the sputtered layer. The layer thickness was additionally confirmed by SEM images of the cross-section of selected samples. These measurements were conducted on a JSM-6300 (JEOL) and a JXA-8530F (JEOL) electron probe microanalyzer (EPMA).

Catalytic Testing: The catalytic measurements were carried out in a dedicated micro-structured clamp reactor fabricated by IMVT and described in^[12] which was adapted to a Microactivity Reference system from PID Eng&Tech. The present reactor, which is applicable up to 523 K and a process pressure of 10 bar, consists of a stack of up to 20 micro-structured foils, where each foil contains 40 parallel reaction channels. The intermetallic layers were sputtered directly into these semi-circular reaction channels having a diameter of 150 μm . For the catalyst pre-treatment, a reduction at 723 K was conducted for 4 h in a quartz glass tube at 40 mL·min⁻¹ flowing Ar/H₂ (5 vol.% H₂ in Ar (> 99.998 %)). The pre-treated foils were loaded in air or inside an Ar filled glovebox into the reactor. Subsequent catalytic tests were conducted for 20 h at 473 K.

The reactants were mixed using Bronkhorst mass flow controllers. The initial gas mixture with a total flow of 40 mL·min⁻¹ consisted of 0.5 vol.% C₂H₂ [Praxair, 99.6 %, 5 vol.% in He (99.996 %)], 5 vol.% H₂ (Praxair, 99.999 %), 50 vol.% C₂H₄ (Westfalen Gas, 99.95 %) and He (Praxair, 99.999 %). A Varian CP 4900 micro gas chromatograph (GC) was used to analyze the product gas stream in a 5 min interval on three columns in parallel. The GC consisted of three modules, each with an individual column and a thermal conductivity detector (TCD). A 5 \AA mol sieves column was used to detect hydrogen and helium from the feed gas as well as nitrogen and oxygen, which are possible impurities resulting from leaks of the experimental set-up. Acetylene, ethylene and ethane were separated on an alumina column. A CP Sil 5 CB column was used to separate the higher hydrocarbons, which are n-butane, 1-butene, *trans*- as well as *cis*-2-butene and 1,3-butadiene. Higher C₆ and C₈ hydrocarbons were not detectable.

For the analysis of the catalytic performance, the conversion of acetylene (C) and the specific activity of the intermetallic nanoparticles (A) were calculated. Additionally, the selectivities to ethylene (S), as well as to C₄ hydrocarbons [$S(\text{C}_4\text{H}_x)$] were determined. The conversion (C) was calculated by the following equation, where φ_{in} and φ_{out} are the volume fractions of acetylene in the feed (in) and in the product stream (out), respectively.

$$C = \frac{\varphi_{\text{in}} - \varphi_{\text{out}}}{\varphi_{\text{in}}} \times 100 \% \quad (4)$$

The activity is applied to compare various catalysts or the same catalyst with different masses or shapes and was calculated according to the following equations:

$$A = \frac{C \dot{n}_{\text{ac}}}{n_{\text{Pd}}} \quad (5)$$

$$\dot{n}_{\text{ac}} = \frac{p \dot{v}_{\text{ac}}}{RT} \quad (6)$$

where n_{Pd} is the total amount of palladium within the nanoparticles and \dot{n}_{ac} is the amount of acetylene in the feed per hour, respectively. The volumetric flow rate \dot{v}_{ac} is converted into the hourly amount of acetylene by using the ideal gas law with the pressure p (1.013 bar), the temperature T (298 K) and the universal gas constant R (8.3144 J·mol⁻¹·K⁻¹). As the catalytic tests were carried out in a very strong excess of ethylene compared to acetylene, the small change of this volume fraction cannot be measured accurately enough and thus, cannot be used to calculate the ethylene selectivity. Additionally, the calculation of this selectivity is based on the assumption that only acetylene, which is hydrogenated to ethylene, can be further hydrogenated to ethane. The selectivities were calculated by the following Equation where φ_{in} and φ_{out} are the volume fractions of acetylene in the feed (in) and in the product stream (out). Additionally, the volume fractions of C₂H₆ and the sum of all C₄ hydrocarbons are required

as these compounds are the main by-products and strongly affect all selectivities:

$$S = \frac{\varphi_{in} - \varphi_{out}}{\varphi_{in} - \varphi_{out} + \varphi_{C_2H_6} + 2 \cdot \varphi_{C_4H_x}} \cdot 100\% \quad (7)$$

$$S_{C_4H_x} = \frac{2 \cdot \varphi_{C_4H_x}}{\varphi_{in} - \varphi_{out} + \varphi_{C_2H_6} + 2 \cdot \varphi_{C_4H_x}} \cdot 100\% \quad (8)$$

Supporting Information (see footnote on the first page of this article): Additional characterization of the sputter target and sputtered films.

Acknowledgements

Financial support from the Deutsche Forschungsgemeinschaft (DFG, German Research Foundation) is acknowledged (grants AR 617/7 and DI 696/11). RZ and MA thank Prof. J. Grin and Dr. H. Borrmann for gratefully providing research facilities as well as substantial assistance with the pXRD measurements at the Max Planck Institute for Chemical Physics of Solids in Dresden, respectively. We thank Dr. U. Burkhardt for the metallographic preparation as well as SEM investigations and Dr. K. Meier-Kirchner for carrying out the SPS experiments.

Keywords: Ethylene; Heterogeneous catalysis; Micro-structured reactor; GaPd₂; PVD

References

- [1] T. E. Nowlin, *Global Polyethylene Business Overview*, in *Business and Technology of the Global Polyethylene Industry*, John Wiley & Sons, Inc.: Hoboken, 2014; pp 1–45.
- [2] A. N. R. Bos, K. R. Westerterp, *Chem. Eng. Process.* **1993**, *32*, 1–7.
- [3] D. Jeremic, *Polyethylene*, in *Ullmann's Encyclopedia of Industrial Chemistry*, Wiley-VCH: 2014; pp 1–42.
- [4] A. Borodziński, G. C. Bond, *Catal. Rev.: Sci. Eng.* **2006**, *48*, 91–144.
- [5] a) D. Teschner, J. Borsodi, A. Wootsch, Z. Revay, M. Hävecker, A. Knop-Gericke, S. D. Jackson, R. Schlögl, *Science* **2008**, *320*, 86–89; b) M. M. Johnson, D. W. Walker, G. P. Nowack, Catalyst, method for the treatment of a gaseous mixture and use of the catalyst for selectively hydrogenating acetylene, 0064301 B1, **1985**.
- [6] a) M. Armbrüster, R. Schlögl, Y. Grin, *Sci. Technol. Adv. Mater.* **2014**, *15*, 034803; b) S. Furukawa, T. Komatsu, *ACS Catal.* **2017**, *7*, 735–765.
- [7] a) K. Kovnir, M. Armbrüster, D. Teschner, T. V. Venkov, F. C. Jentoft, A. Knop-Gericke, Y. Grin, R. Schlögl, *Sci. Technol. Adv. Mater.* **2007**, *8*, 420–427; b) J. Osswald, K. Kovnir, M. Armbrüster, R. Giedigkeit, R. Jentoft, U. Wild, Y. Grin, R. Schlögl, *J. Catal.* **2008**, *258*, 219–227.
- [8] M. Armbrüster, G. Wowsnick, M. Friedrich, M. Heggen, R. Cardoso-Gil, *J. Am. Chem. Soc.* **2011**, *133*, 9112–9118.
- [9] K. Schubert, J. Brandner, M. Fichtner, G. Linder, U. Schygulla, A. Wenka, *Microscale Thermophys. Eng.* **2001**, *5*, 17–39.
- [10] P. Pfeifer, *Application of Catalysts to Metal Microreactor Systems*, in *Chemical Kinetics* (Ed.: V. Patel), InTech: Rijeka, **2012**; pp 325–344.
- [11] a) F. Vidal Vázquez, P. Simell, J. Pennanen, J. Lehtonen, *Int. J. Hydrogen Energy* **2016**, *41*, 924–935; b) A. K. Mogalicherla, S. Lee, P. Pfeifer, R. Dittmeyer, *Microfluid. Nanofluid.* **2013**, *16*, 655–666; c) W. Ehrfeld, V. Hessel, H. Löwe, *Microsystems for Gas Phase Reactions*, in *Microreactors*, Wiley-VCH: Weinheim, **2004**; pp 173–227.
- [12] M. Siebert, R. R. Zimmermann, M. Armbrüster, R. Dittmeyer, *ChemCatChem* **2017**, *9*, 3733–3742.
- [13] R. Dittmeyer, L. Bortolotto, *Appl. Catal. A* **2011**, *391*, 311–318.
- [14] H. F. Guo, M. Kemell, A. Al-Hunaiti, S. Rautiainen, M. Leskela, T. Repo, *Catal. Commun.* **2011**, *12*, 1260–1264.
- [15] P. Panjan, M. Čekada, J. Dolinšek, B. Vrtič, A. Zalar, D. Kek-Merl, *Vacuum* **2008**, *82*, 286–289.
- [16] M. Čekada, J. Dolinšek, P. Panjan, *Vacuum* **2005**, *80*, 137–140.
- [17] a) C. Mathieu, M. J. Hadley, V. R. Inturi, *J. Appl. Phys.* **2008**, *103*, 07E715; b) Y. Fu, X. Cheng, Z. Yang, *Phys. Status Solidi A* **2005**, *202*, 1150–1154; c) M. Abuin, L. Perez, A. Mascaraque, M. Maicas, *CrystEngComm* **2014**, *16*, 9528–9533.
- [18] C. C. Kim, W. H. Kim, J. H. Je, D. W. Kim, H. K. Baik, S. M. Lee, *Electrochem. Solid-State Lett.* **2000**, *3*, 335–337.
- [19] M. Grodzicki, P. Mazur, J. Pers, J. Brona, S. Zuber, A. Ciszewski, *Appl. Phys. A* **2015**, *120*, 1443–1451.
- [20] L. Mayr, H. Lorenz, M. Armbrüster, S. A. Villaseca, Y. Luo, R. Cardoso, U. Burkhardt, D. Zemlyanov, M. Haevecker, R. Blume, A. Knop-Gericke, B. Klötzer, S. Penner, *J. Catal.* **2014**, *309*, 231–240.
- [21] K. Kovnir, M. Schmidt, C. Waurisch, M. Armbrüster, Y. Prots, Y. Grin, *Z. Kristallogr., New Cryst. Struct.* **2008**, *223*, 7–8.
- [22] R. Leary, F. de la Peña, J. S. Barnard, Y. Luo, M. Armbrüster, J. M. Thomas, P. A. Midgley, *ChemCatChem* **2013**, *5*, 2599–2609.
- [23] M. Krajčí, J. Hafner, *ChemCatChem* **2016**, *8*, 34–48.
- [24] J. Osswald, R. Giedigkeit, R. Jentoft, M. Armbrüster, F. Girgsdies, K. Kovnir, T. Ressler, Y. Grin, R. Schlögl, *J. Catal.* **2008**, *258*, 210–218.
- [25] A. Stierle, A. Steinhäuser, A. Rühm, F. U. Renner, R. Weigel, N. Kasper, H. Dosch, *Rev. Sci. Instrum.* **2004**, *75*, 5302–5307.

Received: March 11, 2020

Published Online: ■

R. R. Zimmermann, M. Siebert, S. Ibrahimkutti, R. Dittmeyer,
M. Armbrüster* 1–10

Intermetallic GaPd₂ Thin Films for Selective Hydrogenation
of Acetylene

